Acoustic Testing of the Bell 699 Rotor on the Tiltrotor Test Rig (TTR) in the National Full-Scale Aerodynamics Complex 40- by 80- Foot Wind Tunnel in Conversion and Airplane Configuration

Kelly Shelts*
Graduate Student
Wichita State University
Wichita, KS, USA

Dr. Natasha Schatzman
Aerospace Engineer
NASA Ames Research Center
Moffett Field, CA, USA

ABSTRACT

The Tiltrotor Test Rig (TTR) provides new proprotor testing capabilities to the National Aeronautics and Space Administration (NASA) and the Department of Defense (DoD). A checkout test for the TTR with the 699 proprotor was performed in the National Full-Scale Aerodynamics Complex (NFAC) 40- by 80-Foot Wind Tunnel from 2017 to 2018. Four microphones were placed around the rotor to capture acoustic data. Revolution based acoustic data processing techniques are evaluated for appropriateness in both helicopter and airplane configurations. This paper presents the acoustic data acquired for the rotor in conversion and airplane configuration.

Notation

A	Blade area (ft^2)
C_T	Rotor thrust coefficient, $\frac{T}{\rho A V_{tip}^2}$
C_T/σ	Blade loading coefficient
c	Chord length (ft)
M_{AT}	Advancing tip Mach number, (1+ μ) M_{tip}
M_{tip}	Mach number at blade tip
N_b	Blade Number
OASPL	Overall Sound Pressure Level (dB; reference: 2 x 10-5 Pa)
P_{RMS}	Root Mean Square Pressure
Pref	Reference Sound Pressure (2 x 10-5 Pa)
R	Radius (ft)
RMS	Root Mean Squared
SPL	Sound pressure level (dB; reference: 2×10^{-5} Pa)
RPM	Rotor rotational speed; revolutions per minute
V_{tip}	Rotor blade rotational speed at tip (ft/s)
V_∞	Tunnel velocity (kts)
T	Thrust (lb*f*)
x	Upstream coordinate relative to rotor hub at α_s = 0°, positive[1] into the wind
y	Vertical coordinate relative to rotor hub at α_s = 0°, positive down
z	Lateral coordinate relative to rotor hub at α_s = 0°
α_s	Rotor shaft angle (deg), measured normal to tunnel flow
μ	Advance ratio, $\frac{V_\infty}{V_{tip}}$
σ	Rotor Solidity, $\frac{N_b c R}{\pi R^2}$

Introduction

The Tiltrotor Test Rig (TTR) provides a new proprotor testing capability to conduct technology development, testing and evaluation of new large-scale proprotors for performance, control, loads, and stability in the National Full-Scale Aerodynamics Complex (NFAC). The TTR is designed to accommodate proprotors up to 26 feet in diameter at speeds up to 300 knots, a combination which is unprecedented by other proprotor test rigs. Initial testing of a full-scale proprotor on the TTR was completed in March 2018 with acoustics being one of the program elements (Ref. 1). Various flight conditions were tested, including sweeps of wind tunnel speed, rotor shaft angle, and thrust (Refs. 2 and 3).

This paper discusses wind tunnel acoustic data processing methods, and the significance of these methods on the results for various flight conditions.

Presented at the VFS Aeromechanics for Advanced Vertical Flight Technical Meeting, San Jose, CA, January 21–23, 2020.

*Aerospace Engineer, NASA Langley Research Center, Hampton, VA, USA

Furthermore, results from conversion and airplane configuration are presented.

BACKGROUND

Previous XV-15 rotor acoustic data were acquired in the NFAC 80- by 120-Foot Wind Tunnel in 1996 and 1999 (Refs. 4–8). These tests provided acoustic trends including directionality, rotor shaft angle dependence, and impulsive noise conditions. Both wind tunnel tests had a limited range of data available.

A checkout test for the TTR with the 699 proprotor was performed in the National Full-Scale Aerodynamics Complex (NFAC) 40- by 80-Foot Wind Tunnel from 2017 to 2018 and therefore added to the limited tiltrotor acoustic data set. Acoustic results were previously presented from this test by Schatzman et al. for helicopter configuration flight conditions (Ref. 1).

TEST HARDWARE

The TTR is a horizontal axis test rig mounted in the wind tunnel on a three-strut support system that rotates on the test-section turntable. The turntable can either face the rotor into the wind at high speed (up to 273 knots in the NFAC or design limit of 300 knots) for airplane configuration (α_s = -90º) or fly edgewise at low speed (up to 120 knots) for helicopter configuration (α_s = 0º) (Refs. 2 and 3). Figure 1 shows the downstream view of the TTR in conversion configuration positioned in the NFAC 40- by 80-Foot Wind Tunnel. The test section walls and floor are treated with acoustically absorbent material to reduce acoustic reflections. This provides an absorptivity of greater than 90% at frequencies above 100 Hz (Ref. 9).

Four microphones were placed around the TTR to take acoustic measurements (Figure 1). Microphones 1 and 2 were free-field G.R.A.S 40 AC ½" microphones with a G.R.A.S. 26 AJ ½" preamplifier (Ref. 10). Microphones 3 and 4 were precision surface G.R.A.S. 40 LS ¼" CCP microphones used with a G.R.A.S. AG0002 CCP input adapter (Ref. 10).

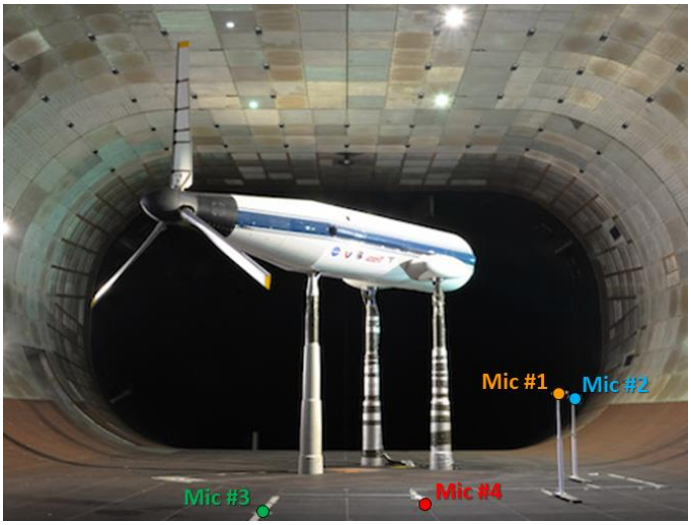

Figure 1. TTR in conversion configuration with microphone locations in the NFAC 40- by 80-Foot Wind Tunnel test section, view looking downstream.

The microphone positions in relation to the hub center are shown in Figure 3 and Table 1. The positive x-direction points upstream, positive y-direction points downward, and positive z-direction is cross-flow. The coordinate system does not change with rotor orientation. Rotor orientation for helicopter, conversion, and airplane configuration are shown in Figure 2.

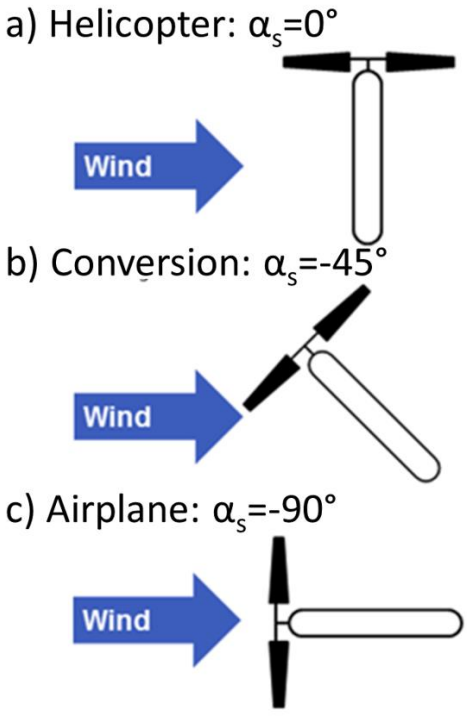

Figure 2. TTR rotor orientation relative to wind direction for a) helicopter, b) conversion, and c) airplane configuration.

The four microphones were positioned near the expected peak Blade Vortex Interaction (BVI) noise directivity angle for helicopter configuration, while ensuring they did not affect the inflow to the rotor in airplane and conversion configuration, see Figure 3.

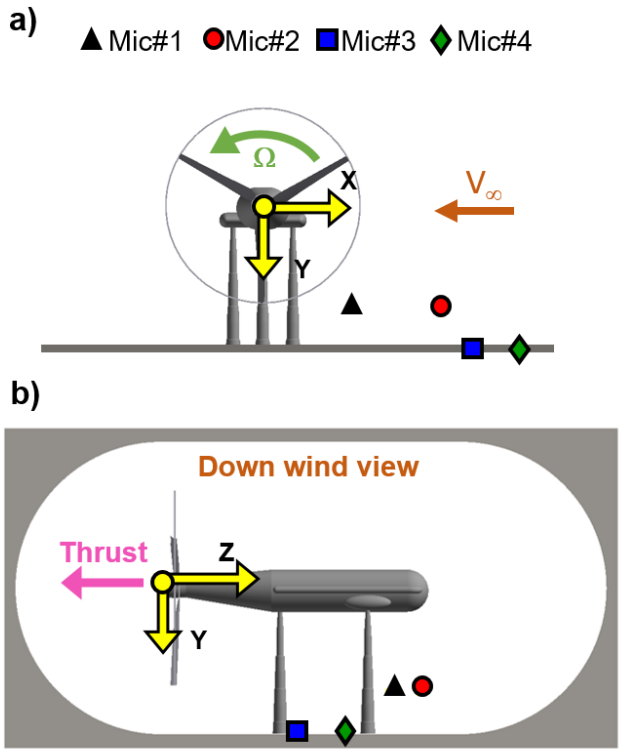

Figure 3. Microphone locations for acoustic measurements of the Bell 699 Rotor on the TTR in the NFAC 40- by 80-Foot Wind Tunnel shown in proximity to the TTR itself in helicopter configuration (α_s = 0º).

Table 1. Microphone positions for the TTR test in the NFAC 40- by 80-Foot Wind Tunnel, with respect to center of hub (α_s = 0º).

Mic #	X/R	Y/R	Z/R	Distance (R)
1	1.9	1.1	2.2	3.03
2	0.9	1.1	2.5	2.84
3	2.7	1.5	1.1	3.27
4	2.2	1.5	1.5	3.06

Mic #	Azimuth (deg)	Elevation (deg)
1	150	45
2	131	60
3	150	20
4	144	30

DATA INSTRUMENTATION AND ACQUISITION

Acoustic data recording setup and components, including preamplifier, calibrator, and data collection systems are shown in Figure 4.

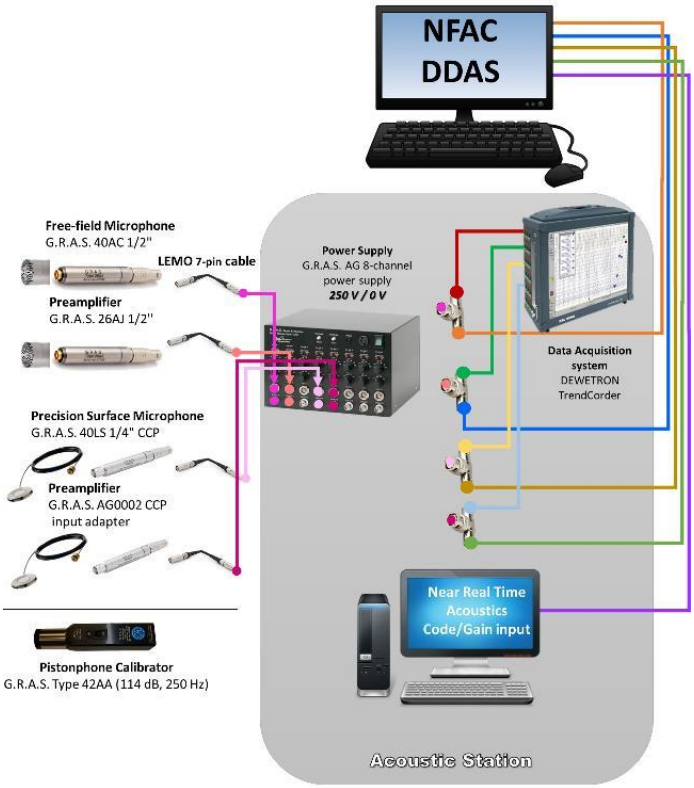

Figure 4. NFAC 40- by 80-Foot Wind Tunnel acoustic data collection setup.

Data was collected with the NFAC Data Acquisition system, DDAS, as well as the NASA supplied Dewetron DAQ. The additional data acquisition system from NASA has a higher sampling rate, ideal for acoustic measurements to capture sound at higher frequencies. To ensure consistency between the two systems, a start trigger, 1/rev signal, and 2048/rev signal were sent from the NFAC DDAS to the Dewetron Trendcorder. These signals were used in data post processing to correlate the data.

The data acquired from the DDAS was collected at a rate of 2048 samples per revolution (19,456 Hz at 570 RPM). This was the sample rate used for the plots in this paper. The Dewetron collects data at a rate of 50 kHz.

TEST CONDITIONS

Background noise was acquired by collecting acoustic data without the Bell 699 rotor on the TTR spinning. The tunnel fan drive system was turned on to evaluate the noise caused by air flow over the test hardware, as well as from the tunnel drive system itself. Rotor-on testing included multiple sweeps of α_s, μ, M_{AT}, and C_T/σ.

This paper focuses on conversion and airplane configurations. Conversion configuration flight includes shaft angles between -10 and -80º. Airplane configuration includes angles between -80 and -100º.

DATA POST PROCESSING TECHNIQUES

Raw acoustic data was converted from volts to acoustic pressure by using the individual microphone calibration constant and microphone gain setting. The acoustic pressure time history was then harmonically averaged. The 1/rev and n/rev signals are used to identify the beginning of each revolution and rotor azimuthal location, respectively. The revolutions are then averaged to create a single time history representative of all 128 revolutions. Two methods are used to calculate overall sound pressure level (OASPL): one from the Fast Fourier Transform (FFT) of the averaged time history and the other from the RMS pressure calculated from the averaged time history (Figure 5). The two methods produce no significant difference in OASPL (less than 0.01% difference for cases presented in this paper).

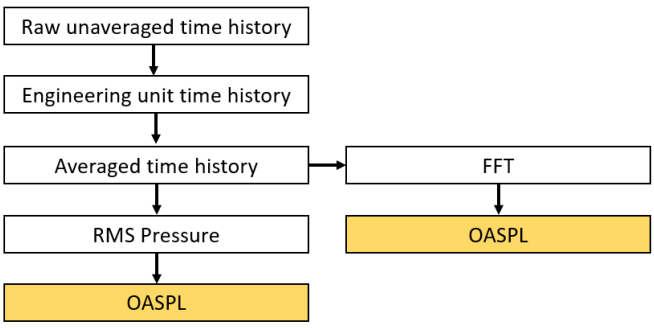

Figure 5. Bell 699 on the TTR in the NFAC 40- by 80- Foot Wind Tunnel acoustic data post-processing procedure.

Using the RMS method, OASPL is calculated using

$$OASPL = 20\ log_{10}(\frac{P_{RMS}}{P_{ref}})$$

Where P_{RMS} is the root-mean-squared pressure over the averaged time history and P_{ref} is the sound pressure threshold of human hearing (Ref. 11).

The sound pressure time history exhibits blade dependence for cases in airplane and helicopter configuration as shown in Figure 6. For a three-bladed rotor, there are three spikes between azimuth 0 and 360º.

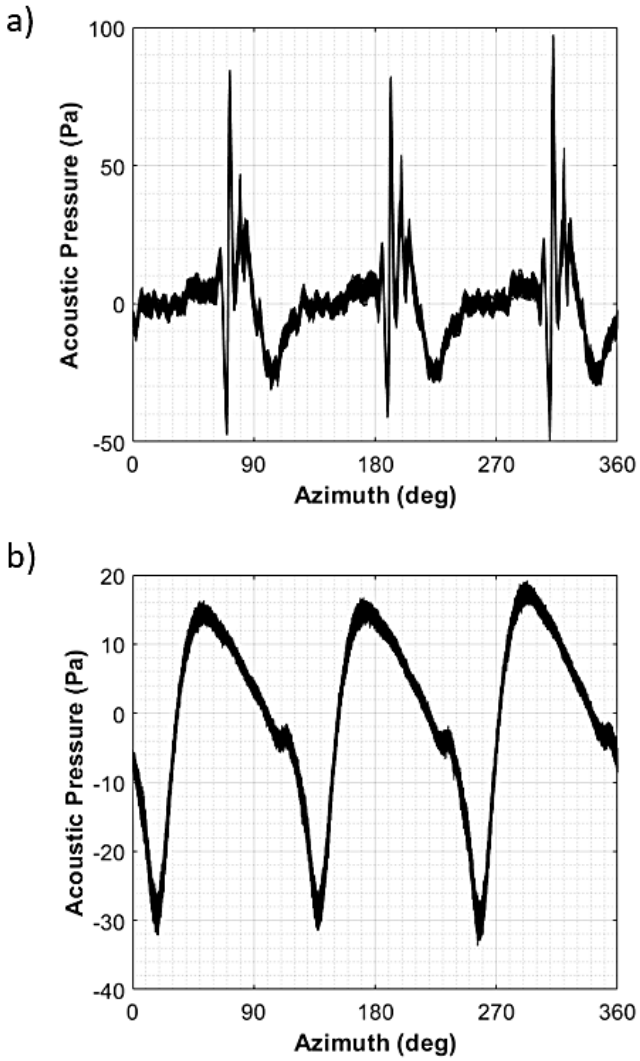

Figure 6. Acoustic time history for 128 revolutions for helicopter (μ = 0.125, C_T/σ = 0.075, α_s = 0º) and b) airplane configuration (μ = 0.033, C_T/σ = 0.055, α_s = -90º).

The traditional processing technique of rotorcraft acoustic data involves creating an averaged time history, referred to as harmonic averaging. With this method, all 128 revolutions are averaged to create a single time history to be used in further analysis. An FFT is performed to show the frequencies of noise that occur. Harmonic averaging is used to reduce the effect of

background noise by focusing on the harmonic noise created during each revolution.

Figure 6 shows 128 revolutions of data for airplane and helicopter configuration for flight conditions of μ = 0.033, C_T/σ = 0.055, α_s = -90º and μ = 0.125, C_T/σ = 0.075, α_s = 0º, respectively**.** Due to the variation from revolution-to-revolution, the data was further analyzed. When an FFT was performed over each revolution, the sound pressure was higher than the FFT of the averaged spectrum (Figure 7). The individual revolution FFT's are shown in various colors, and the averaged spectrum FFT is shown in black. This occurred in both helicopter and airplane configuration.

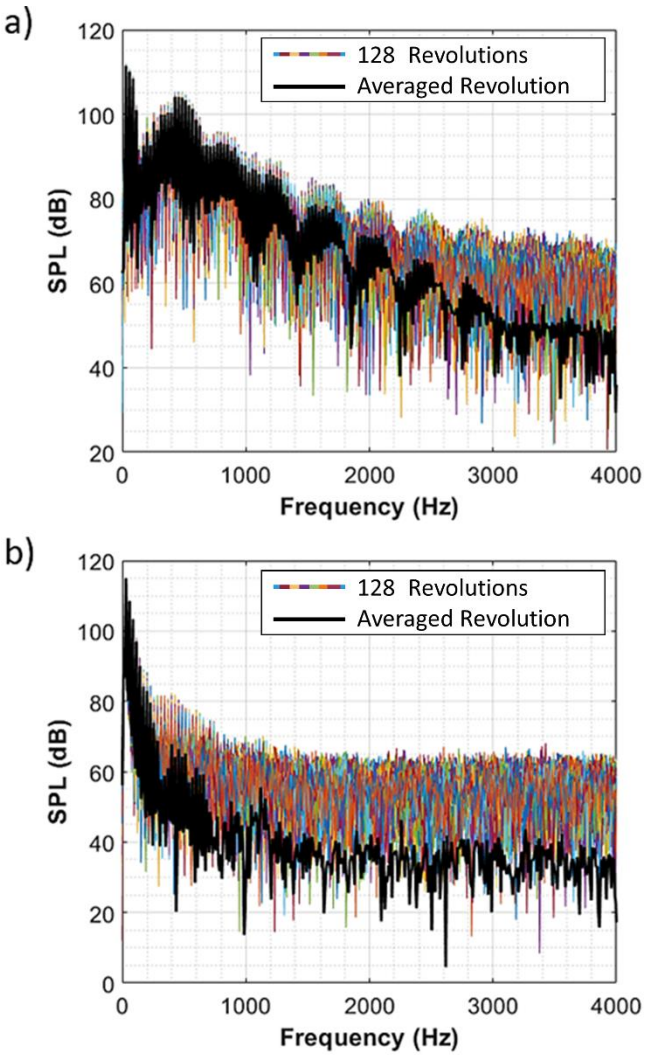

Figure 7. Individual revolution frequency spectrum and averaged pressure frequency spectrum for a) airplane condition (μ = 0.033, C_T/σ = 0.055, α_s = -90º) and b) helicopter configuration (μ = 0.125, C_T/σ = 0.075, α_s = 0º).

The following analyses were performed to investigate the variance between revolutions and ensure that the averaging techniques were not significantly affecting the final acoustic results.

Peak-to-peak Evaluation

The next analysis evaluated the pulse maximum and minimum that occur for each blade revolution. Each rotor revolution produced a similar pressure trend but resulted in different peak pressure values. In Figure 8, the first blade dependent peak was considered for both airplane and helicopter configuration. The maximum and minimum pressure values and revolution number in which they occurred are shown. The individual revolutions were analyzed to determine the variance in peak-to-peak acoustic pressure values.

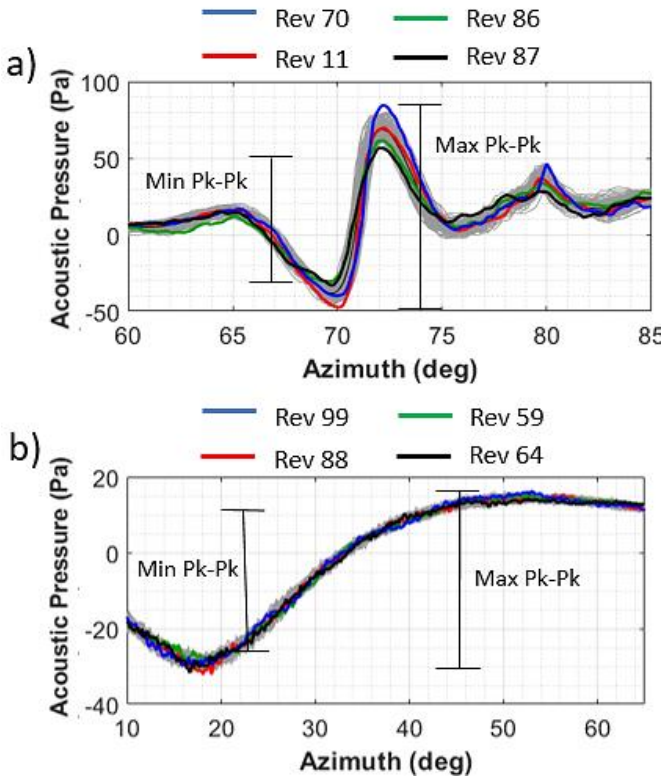

Figure 8. Peak-to peak variation for a) helicopter (μ = 0.125, C_T/σ = 0.075, α_s = 0º) and b) airplane configuration (μ = 0.033, C_T/σ = 0.055, α_s = -90º) for blade 1.

In helicopter configuration, the peak-to-peak pressure values have less than 25% difference from the 128-revolution average peak pressure. In airplane configuration, the peak-to-peak values have less than 7% difference from the 128-revolution average peak pressure. Peak-to-peak values change between the blades (Figure 9 and 10).

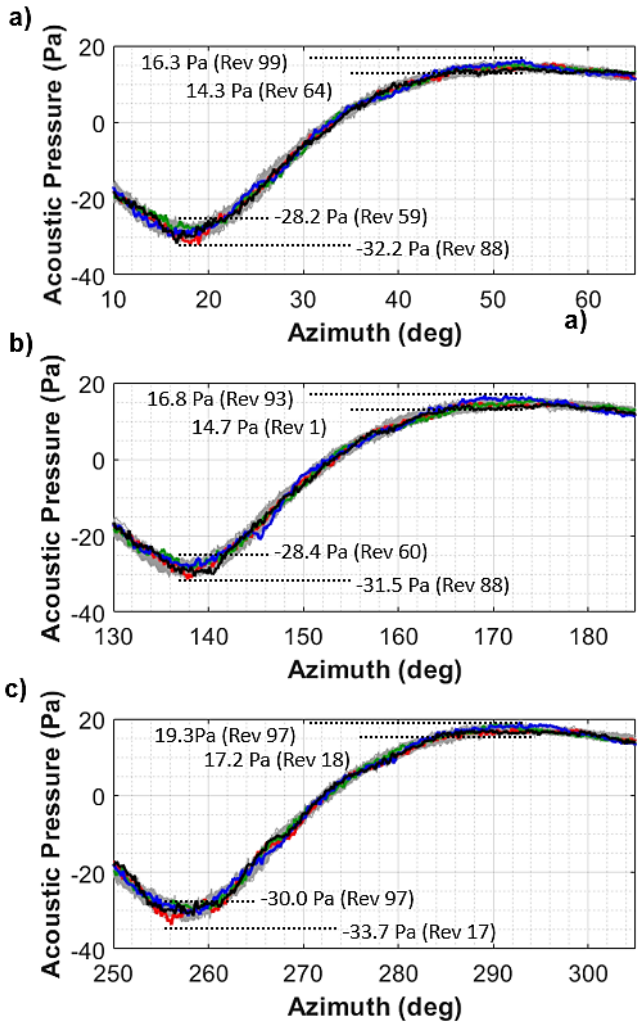

Figure 9. Peak-to-peak variation for helicopter configuration ($\mu = 0.125$, $C_T/\sigma = 0.075$, $\alpha_s = 0^o$) for a) blade 1, b) blade 2, and c) blade 3.

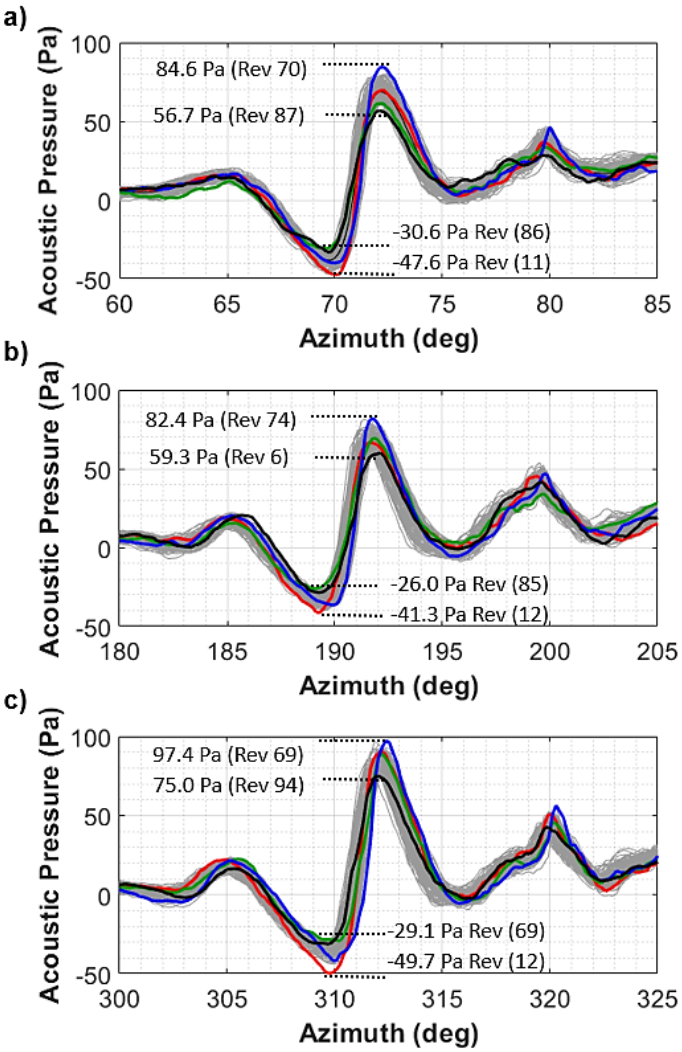

Figure 10. Peak-to-peak variation for airplane configuration ($\mu = 0.033$, $C_T/\sigma = 0.055$, $\alpha_s = -90^o$) for a) blade 1, b) blade 2, and c) blade 3.

The peak pressure values occur during different revolutions for both airplane and helicopter configuration. The amount of spread does not change significantly between the blades (Figures 9 and 10).

Further investigation is needed to account for these pressure differences. As presented in the revolution averaging section, the OASPL did not significantly differ revolution to revolution.

Evaluation of RPM Variation

To further check test validity, RPM was calculated for each run in both airplane and helicopter configuration. The statistics are presented in Table 2. There was no significant change in RPM throughout the test. RPM variation is not the cause for acoustic differences between revolutions.

Table 2. RPM statistics for helicopter and airplane configuration.

Case	Min	Max	Std Dev
Helicopter configuration ($\mu = 0.125$, $C_T / \sigma = 0.075$, $\alpha_s = 0°$)	569.26	569.69	.1008
Airplane configuration ($\mu = 0.033$, $C_T / \sigma = 0.055$, $\alpha_s = -90°$)	568.94	569.37	.1058

Peak Relocation Evaluation

The azimuth location of the peak pressure value varies slightly in individual revolutions. This may be due, in part, to the variation in RPM. When harmonically averaging, the dislocation may cause the acoustic pressure time history to have lower amplitude peaks. For each revolution, the data was shifted to ensure that the peak pressure value occurred at the same azimuthal location (Figure 11). Then, the data averaged and OASPL was calculated.

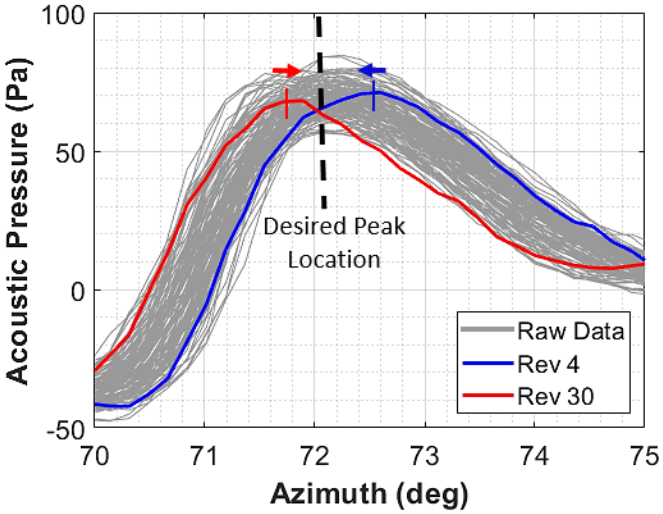

Figure 11. Peak movement for helicopter configuration ($\mu = 0.125$, $C_T/\sigma = 0.075$, $\alpha_s = 0^o$).

The results of peak shifting for blade 1 peak 1 in helicopter configuration are shown in Figure 12.

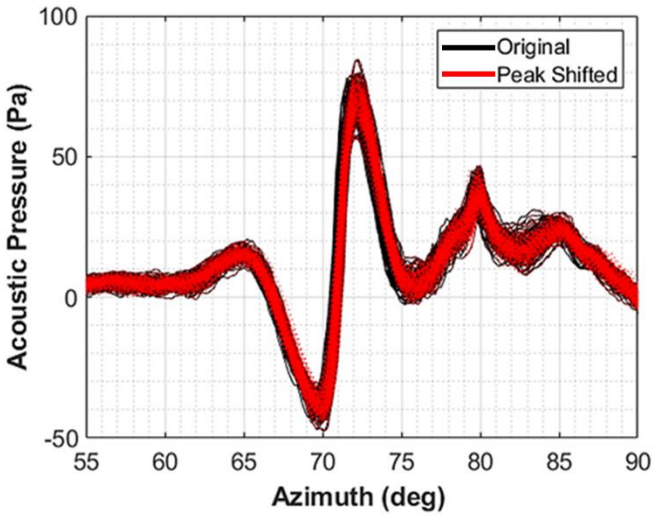

Figure 12. Peak movement for helicopter configuration ($\mu = 0.125$, $C_T/\sigma = 0.075$, $\alpha_s = 0^o$).

The peak movement resulted in a difference of 0.2% in OASPL for helicopter configuration. The same analysis was performed for airplane configuration (Figure 13). The peak movement did not change the OASPL calculated for airplane configuration. Peak relocation did not result in any significant changes for both helicopter and airplane mode for these flight conditions.

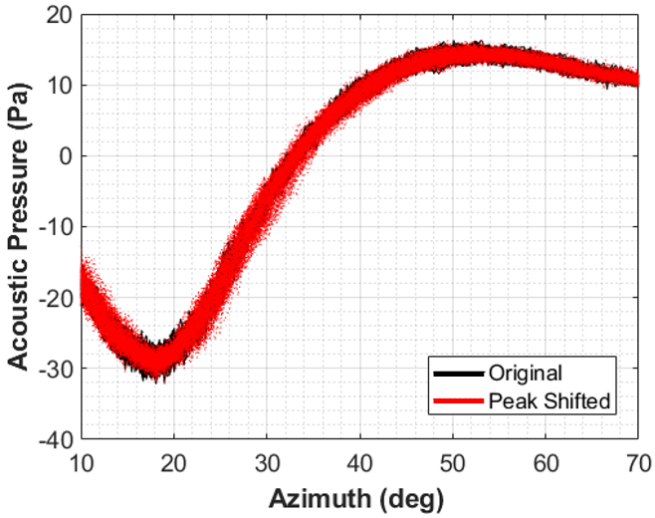

Figure 13. Peak movement for airplane configuration ($\mu = 0.033$, $C_T/\sigma = 0.055$, $\alpha_s = -90^o$).

Evaluation of Revolution Averaging

Schatzman et al. presented the averaged time history and each individual revolution as shown in Figure 14a. The averaged data is shown in red and the individual revolutions are shown in gray of a sample acoustic time history. The background noise is also shown in Figure

14a, for 60 knots, $\alpha_s = 0^o$, blades off, where the blue is the averaged time history and the black is all 128 revolutions. The averaged data is smoother than the individual revolutions. Harmonic averaging greatly reduced background noise (Figure 14a).

Differences between the averaged data and unaveraged data were further investigated by comparing the frequency spectrum (Figure 14b). Averaging all 128 revolutions reduces the amount of high frequency noise in the spectrum. The averaged data is lower in magnitude than the unaveraged data, especially at higher frequencies. Averaging removes some of the random noise generated, reducing the overall acoustic pressure magnitude.

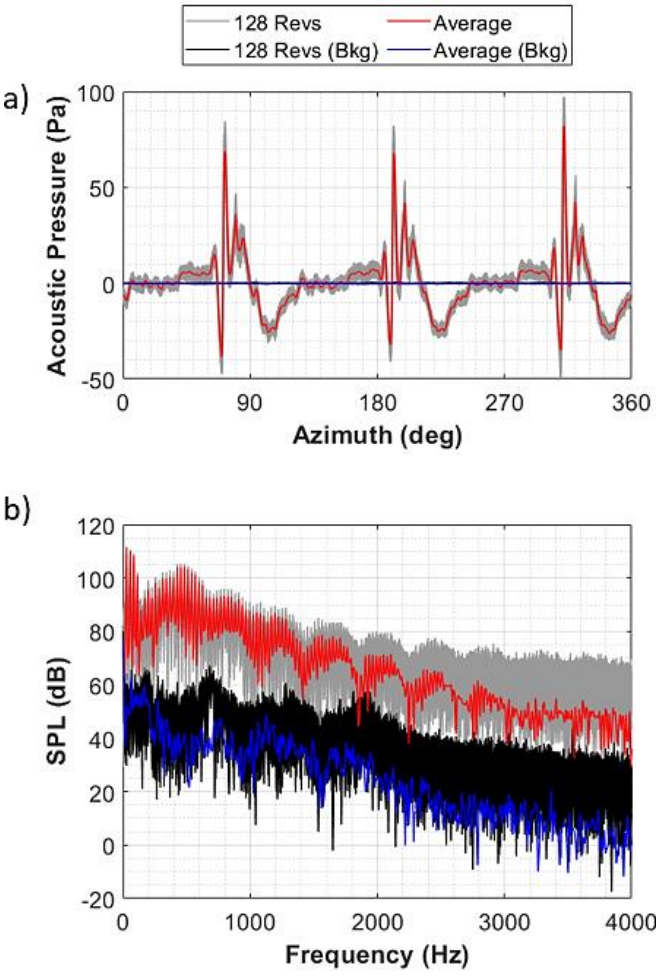

Figure 14. a) Averaged and unaveraged acoustic time history, b) averaged and unaveraged data in frequency domain ($\mu = 0.125$, $C_T/\sigma = 0.075$, $M_{AT} = 0.770$, and $\alpha_s = 0^o$).

Figure 15a shows a single pulse from the acoustic time history for the harmonically averaged data and a single revolution of data. The single, unaveraged revolution of data (grey) shows a less smooth acoustic signature compared to the averaged acoustic data. This shows how higher frequencies were averaged out. Furthermore, the background noise from the unaveraged revolution of data (black) shows a less smooth acoustic signature compared to the averaged acoustic data (blue). A single revolution of data contains more high frequency content than the averaged data (Figure 15b). This high frequency content was averaged out in the harmonic averaging process. This did not significantly affect the OASPL calculated.

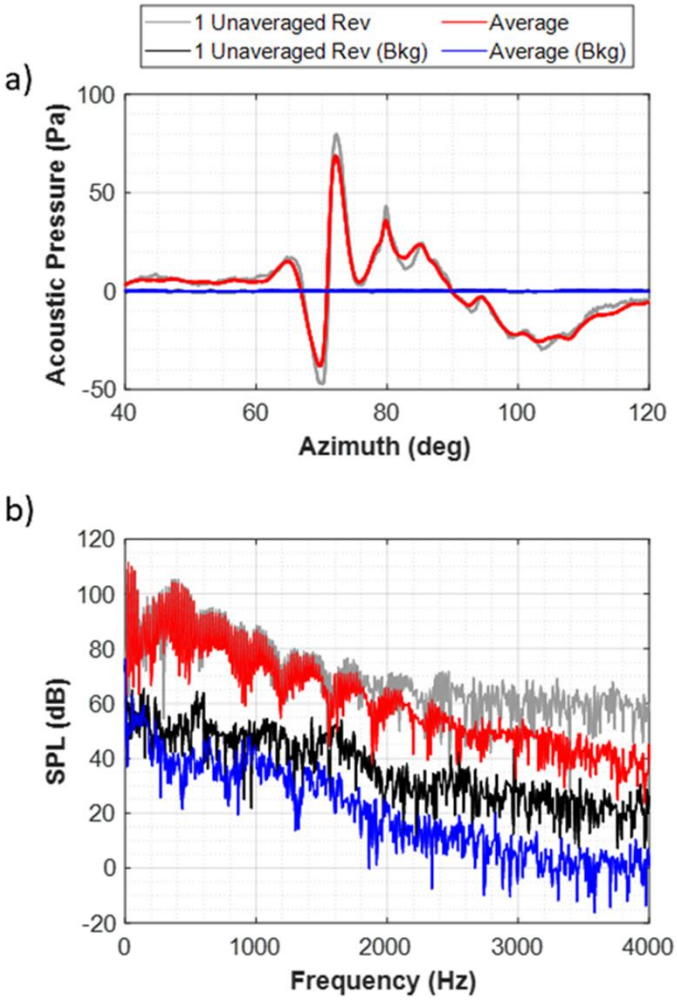

Figure 15. Averaged acoustic data for an averaged and a single revolution a) time history and b) frequency spectrum for microphone 1 for a flight condition of $C_T/\sigma = 0.075$, $\mu = 0.125$, $M_{tip} = 0.684$, $M_{AT} = 0.770$, and $\alpha_s = 0^o$ and background noise of 60 knots, $\alpha_s = 0^o$, blades off.

The same trends are shown in airplane configuration (Figure 16 and 17).

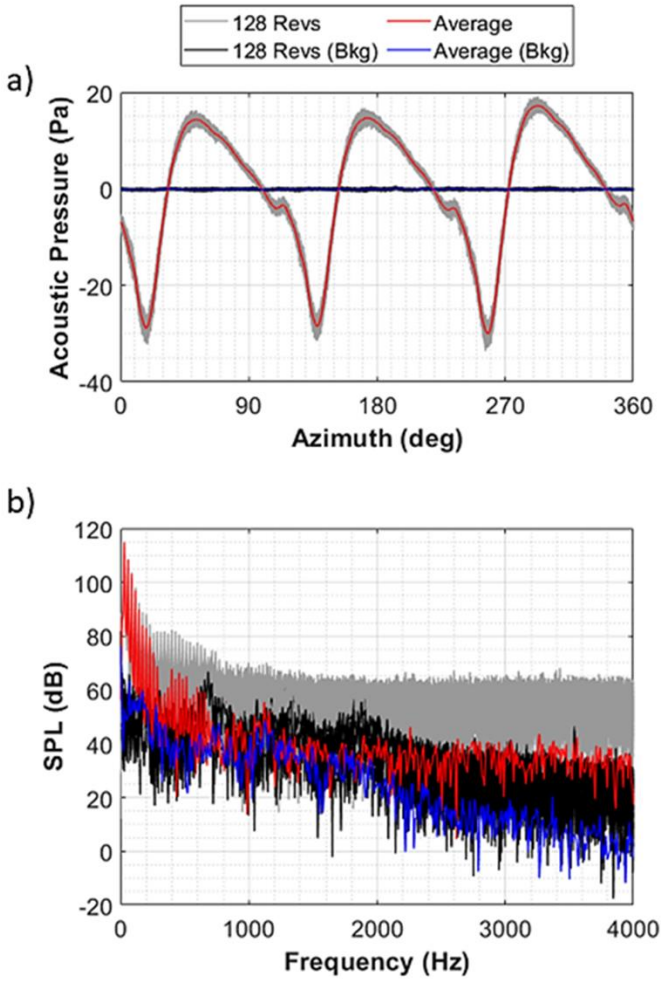

Figure 16. a) Averaged and unaveraged acoustic time history, b) averaged and unaveraged data in frequency domain (μ = 0.033, C_T/σ = 0.055, M_{tip} = 0.684, M_{AT} = 0.770, and α_s = -90º)

There is less variation between the revolutions in airplane than helicopter configuration (Figure 17). Averaging reduces the SPL at all frequencies, removing background noise.

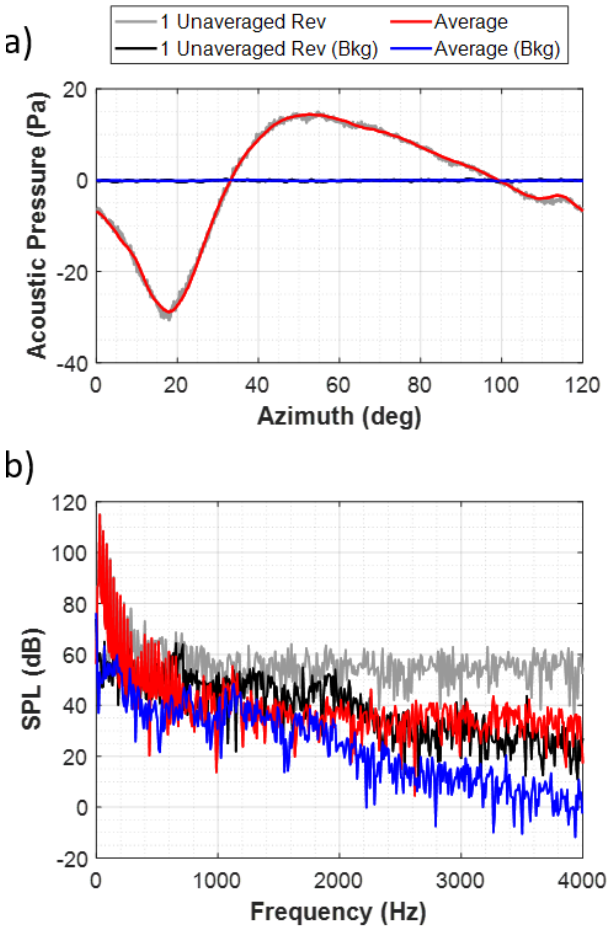

Figure 17. Averaged acoustic data for an averaged and a single revolution a) time history and b) frequency spectrum for microphone 1 (μ = 0.033, C_T/σ = 0.055, M_{tip} = 0.684, M_{AT} = 0.770, and α_s = -90º) and background noise of 60 knots, α_s = 0º.

To evaluate how OASPL varies from revolution to revolution, the OASPL was calculated for each revolution and then averaged, as shown below

$$OASPL = mean\,(20\,log_{10}\left(\frac{\vec{P}}{P_{ref}}\right))$$

In helicopter configuration, the difference between this method and the OASPL from the averaged time history was 0.26%. In airplane configuration, this difference was 1.03%.

FFT Averaging

A revolution averaged acoustic spectrum can be acquired two different ways: by averaging the sound pressure data for each revolution and then taking the FFT or by taking the FFT of each revolution then averaging the FFT

results. These produce different results, as shown in Figure 18. Averaging the FFT's produces a result similar to an individual revolution FFT (revolution number 15 selected for example). It doesn't filter out as much of the background noise as harmonic averaging before the FFT is taken.

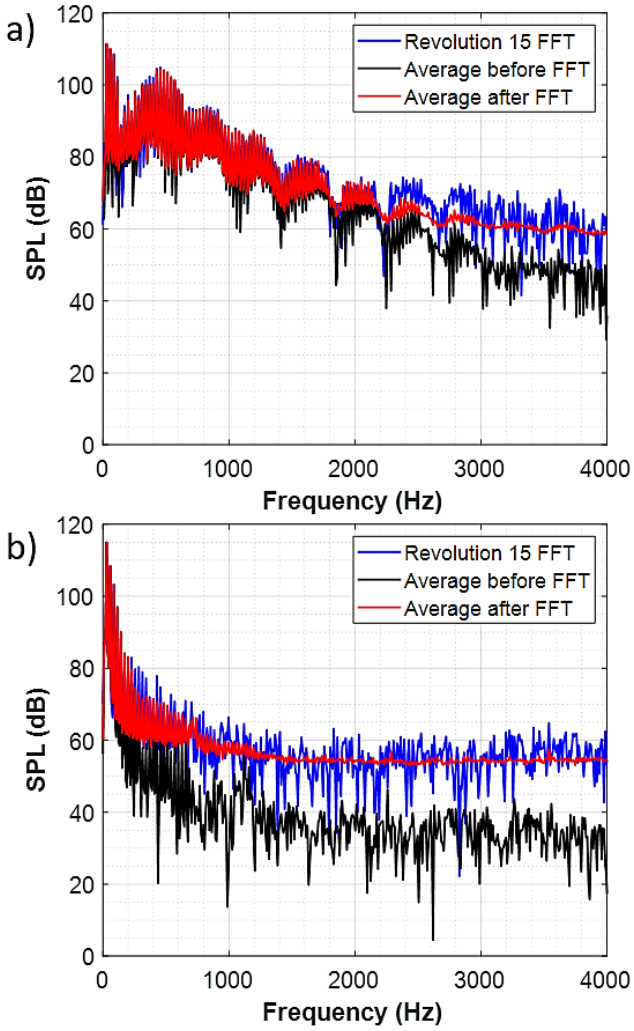

Figure 18. Averaged acoustic spectrum with averaging done before and after FFT for flight condition of a) C_T/σ = 0.075, μ = 0.125, M_{tip} = 0.684, M_{AT} = 0.770, and α_s = 0° and b) C_T/σ = 0.055, μ = 0.126, M_{tip} = 0.689, M_{AT} = 0.712, and α_s = -90°.

There was no significant change in OASPL from any of the post processing methods considered, supporting the validity of the traditional harmonically averaging time history method for OASPL calculation. Averaging reduces the contribution of non-rotor (harmonic) related noise. The individual spectrum has higher sound pressure levels (Figure 18) because the non-rotor noise is not averaged out.

DATA QUALITY

Data quality was evaluated by analyzing background noise in the NFAC 40-by 80-Foot Wind Tunnel, as well as result repeatability. Result repeatability was evaluated by looking at all revolutions of data, and by comparing the acoustic time histories between the three blades.

A comparison between background and rotor-on noise is shown in Figure 19 for airplane configuration. Mic 1 measured an OASPL of 116.1 dB and the background OASPL was 74.9 dB, resulting in an adequate signal to noise ratio.

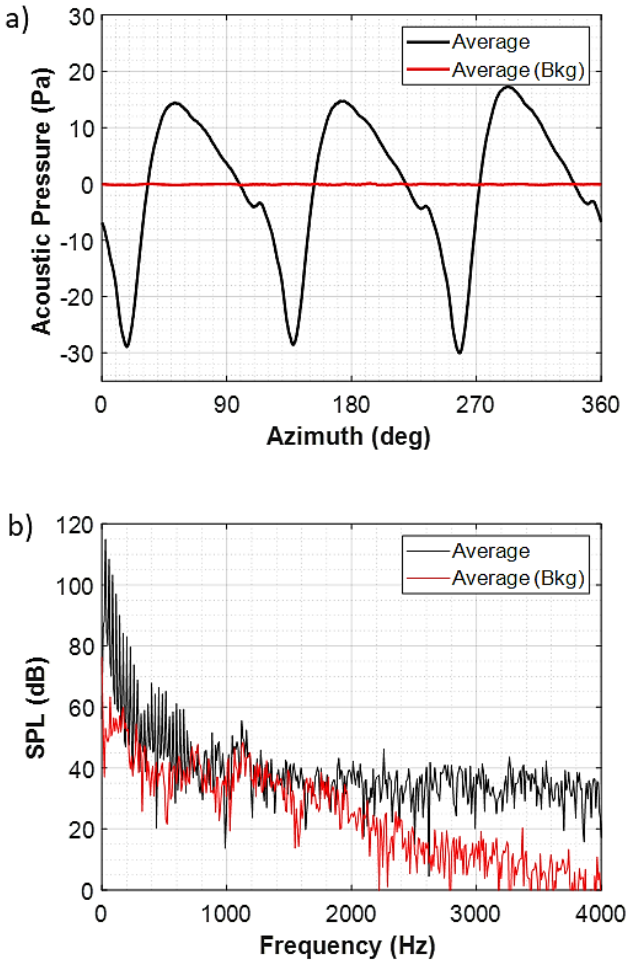

Figure 19. a) Averaged acoustic time history and b) frequency spectrum of background noise (90 knots, α_s = -90°, blades off) and at a flight condition in airplane configuration (μ = 0.0328, C_T/σ = 0.055, α_s = -90°).

A comparison between background and rotor-on noise is shown in Figure 20 for conversion configuration. Mic 1

measured an OASPL of 110.8 dB with a background of 74.3 dB, resulting in an adequate signal to noise ratio.

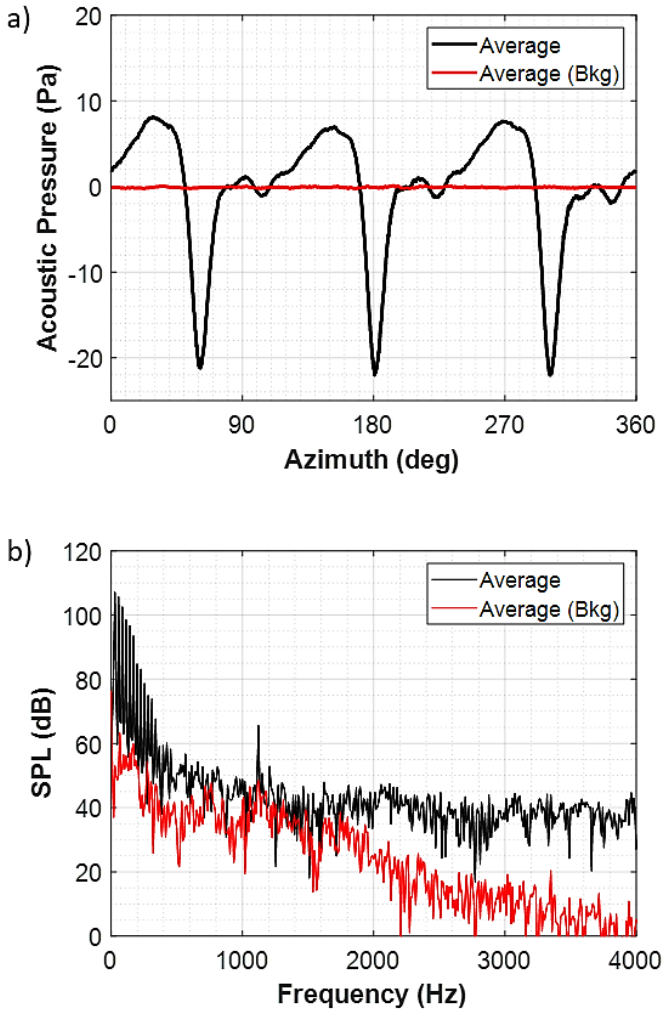

Figure 20. a) Averaged acoustic time history and b) frequency spectrum of background noise (90 knots, α_s = -60º, blades off) and at a flight condition in conversion configuration (μ = 0.125, C_T/σ = 0.049, α_s = -44.8º).

Data repeatability was evaluated by comparing the averaged time history to the individual revolution time history. Figure 21 shows minimal acoustic pressure variation between revolutions.

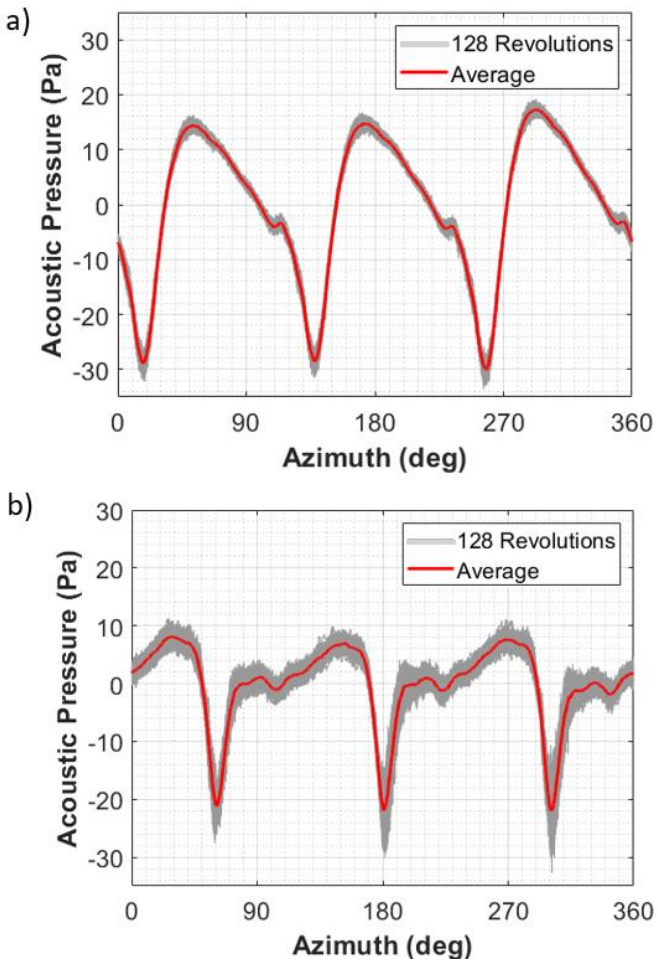

Figure 21. Acoustic time history for a) airplane (μ = 0.0328, C_T/σ = 0.055, α_s = -90º) and b) conversion configuration (μ = 0.125, C_T/σ = 0.049, α_s = -44.8º).

Blade-to-blade differences were evaluated as seen in Figure 22. For airplane and helicopter configuration, the first pulse occurs from azimuth angles 0º to 120º, the second from 120º to 240º, and the third from 240º to 360º. There were minimal differences between each blade.

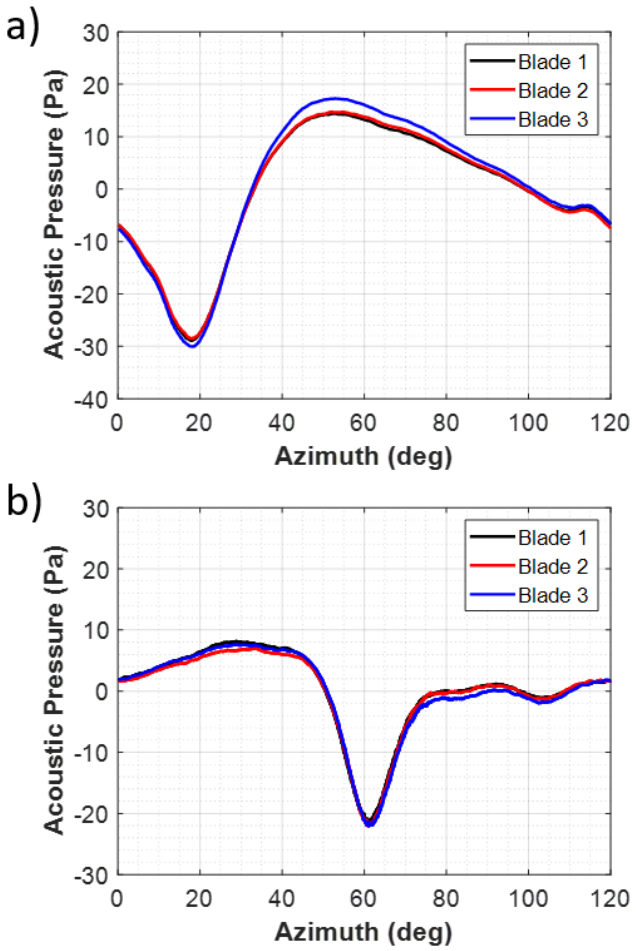

Figure 22. Blade-to-blade comparison for a) airplane a) airplane (μ = 0.0328, C_T/σ = 0.055, α_s = -90º) and b) conversion configuration (μ = 0.125, C_T/σ = 0.049, α_s = -44.8º).

RESULTS AND DISCUSSION

Acoustic time histories and OASPL trends are presented for selected flight conditions. A rotor shaft angle sweep is presented from helicopter to airplane configuration. A thrust and advancing tip Mach number sweep is performed for conversion and airplane configuration.

Figure 23 shows averaged acoustic time histories for microphone 1 at various shaft angels for a M_{tip} of 0.684 and V_∞ of 60 kts. These results have not been corrected for varying distance to microphone 1 at the different rotor shaft angles.

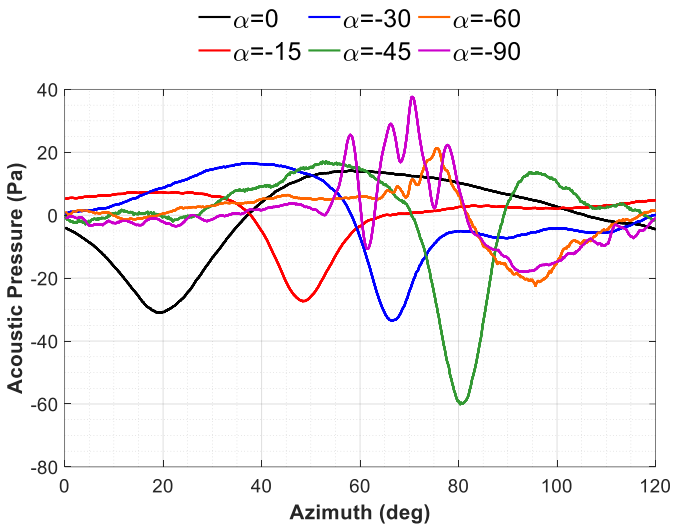

Figure 23. Averaged acoustic time history for microphone 1 at various rotor shaft angles (M_{tip} = 0.684 and V_∞ = 60 kts).

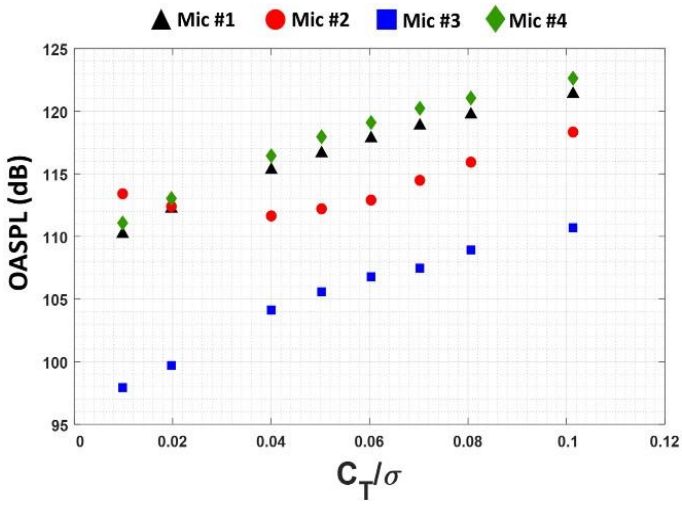

Figure 24. OASPL versus C_T/σ for microphones 1 through 4 for an airplane configuration condition of μ = 0.132, M_{tip} = 0.684, M_{AT} = 0.775, and α_s = -90º.

Figure 24 shows OASPL versus C_T/σ for microphones 1 through 4 for an airplane configuration condition of μ = 0.132, M_{tip} = 0.684, M_{AT} = 0.775, and α_s = -90º. For all four microphones, OASPL increased as thrust increased. In Figure 25, the acoustic time history is shown for various thrust values for microphone 1. Peak-to-peak pressure difference increases with thrust.

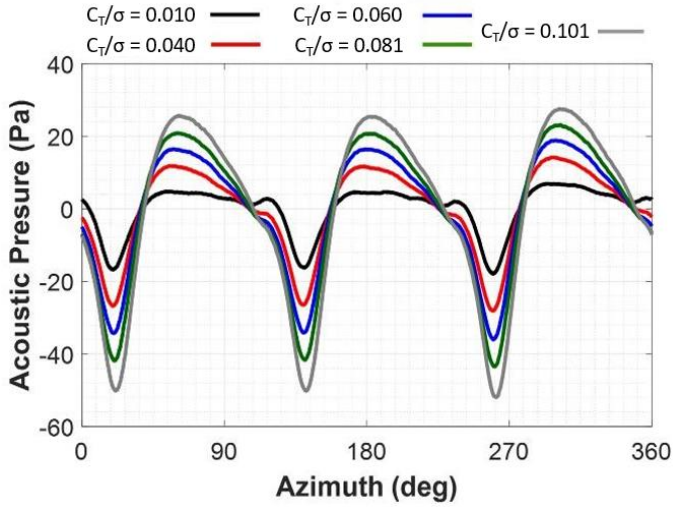

Figure 25. Averaged acoustic time history for microphone 1 for an airplane configuration condition of various C_T/σ for μ = 0.132, M_{tip} = 0.684, M_{AT} = 0.775, and α_s = -90º.

A sweep of advancing tip Mach number is shown for a flight condition in airplane configuration of C_T/σ = 0.039, and α_s = -90º in Figure 26. This is done by increasing the wind speed within the tunnel. As advancing tip Mach number increased so did OASPL.

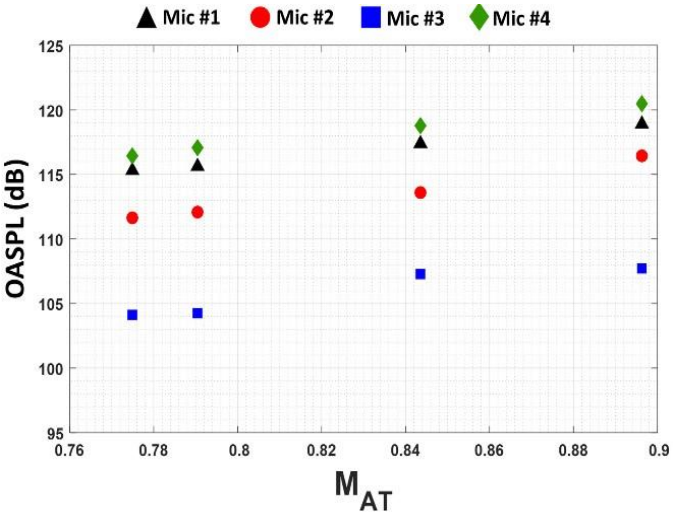

Figure 26. OASPL versus M_{AT} for microphones 1 through 4 for an airplane configuration condition of C_T/σ = 0.039, α_s = -90º, and M_{tip} = 0.684.

OASPL increased with increasing M_{AT} for all four microphones. Figure 27 shows the acoustic time history for various M_{AT} values for microphone 1. Higher M_{AT} values correspond to higher peak-to-peak sound pressure values.

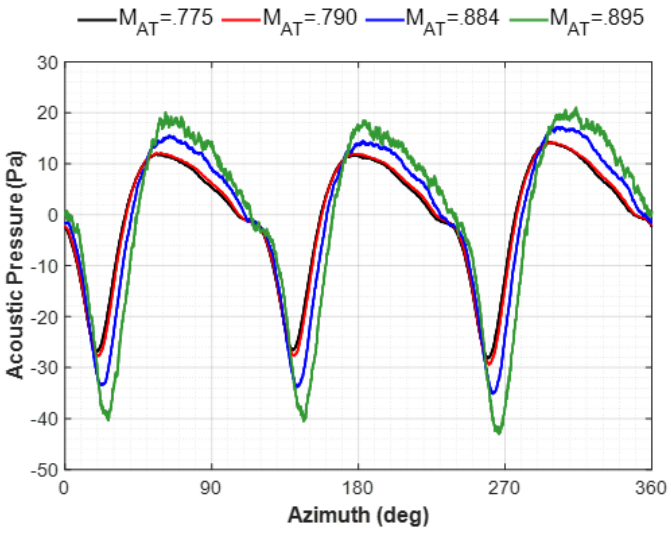

Figure 27. Averaged acoustic time history for microphone 1 for an airplane configuration condition of C_T/σ = 0.039, α_s = -90º, and M_{tip} = 0.684.

Figure 28 shows OASPL versus C_T/σ for microphones 1 through 4 for μ = 0.152, M_{tip} = 0.684, M_{AT} = 0.786, and α_s = -30º. As shown in Figure 26 for airplane configuration, the OASPL increased with increasing thrust for all microphones for conversion configuration.

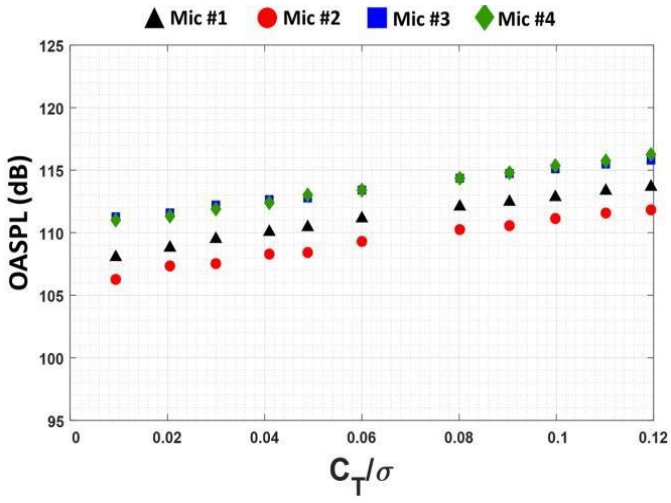

Figure 28. OASPL versus C_T/σ for microphones 1 through 4 for a conversion configuration condition of μ = 0.152, M_{tip} = 0.684, M_{AT} = 0.786, and α_s = -30º.

Figure 29 shows the acoustic time history for varying C_T/σ values. The peak-to-peak sound pressure level increased with increasing thrust.

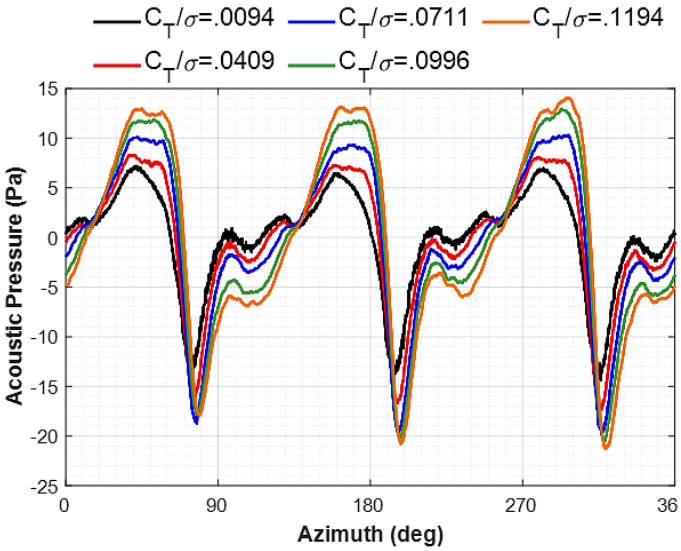

Figure 29. Averaged acoustic time history microphone 1 for a conversion configuration condition of $\mu = 0.152$, $M_{tip} = 0.684$, $M_{AT} = 0.786$, and $\alpha_s = -30^o$.

A sweep of advancing tip Mach number is shown for the conversion configuration flight condition of $C_T/\sigma = 0.021$, and $\alpha_s = -30^o$ is shown in Figure 30. Again, as seen for airplane configuration (see Figure 26), an increase in advancing tip Mach number resulted in an increase in OASPL for all microphones.

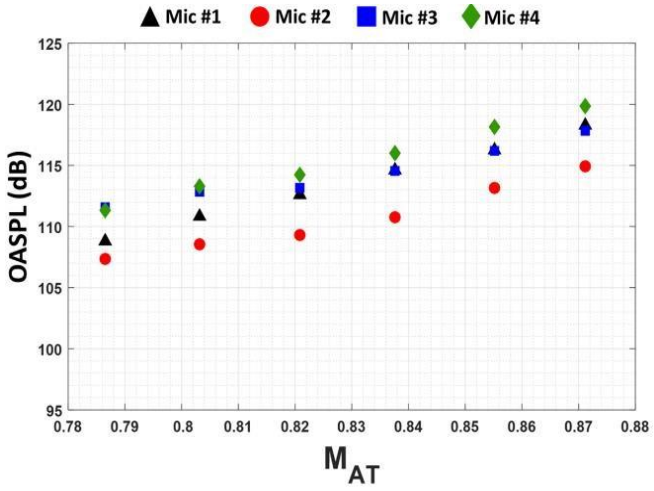

Figure 30. OASPL versus M_{AT} for microphones 1 through 4 for a conversion configuration condition of $C_T/\sigma = 0.021$, $\alpha_s = -30^o$, and $M_{tip} = 0.684$.

Similarly, higher M_{AT} corresponds to higher peak-to-peak sound pressure levels in conversion configuration (Figure 31).

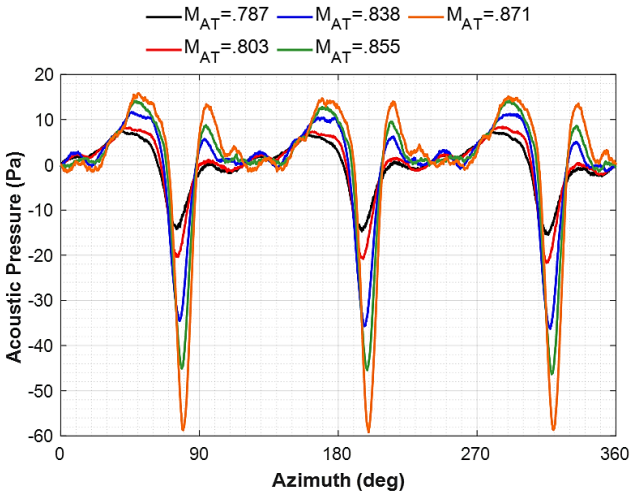

Figure 31. Averaged acoustic time history microphone 1 for a conversion configuration condition of $C_T/\sigma = 0.021$, $\alpha_s = -30^o$, and $M_{tip} = 0.684$.

CONCLUDING REMARKS

The TTR checkout test with the Bell 699 installed was completed in 2018, and acoustic measurements were taken during this test for helicopter, conversion, and airplane configuration.

The processing technique of harmonic averaging was investigated for helicopter and airplane configuration for selected flight conditions. This investigation included performing a peak relocation for each revolution, though the presented technique did not did not produce significant change in OASPL. Furthermore, a comparison of time history and spectrum between individual revolutions and the averaged revolution were discussed.

Acoustic time histories were presented for airplane and conversion configuration flight conditions. OASPL increased with increasing thrust and advancing tip Mach number for both airplane and conversion configurations.

ACKNOWLEDGEMENTS

We would like to acknowledge Dr. Ben Wel-C. Sim. Dr. Sim participated in the acoustic set up and recording of the acoustic data in the NFAC 40- by 80-Foot Wind Tunnel.

REFERENCES

[1] Schatzman, N.L. and Malpica, C., "Acoustic Testing of the Tiltrotor Test Rig in the National Full-Scale Aerodynamics Complex 40- by 80- Foot Wind Tunnel," Vertical Flight Society 75th Annual Forum, Philadelphia, PA, 2019.

[2] Acree, C. W., Sheikman A. L., and Norman T. R., "High Speed Wind Tunnel Tests of a Full-Scale Proprotor on the Tiltrotor Test Rig," Vertical Flight Society 75th Annual Forum, Philadelphia, PA, 2019.

[3] Kottapalli, S., and Acree, C. W., "Correlation of Full Scale Isolated Proprotor Performance and Loads," Vertical Flight Society 75th Annual Forum Proceedings, Philadelphia, PA, 2019.

[4] Young L., "Tilt Rotor Aeroacoustic Model (TRAM): A New Rotorcraft Research Facility", International Meeting on Advanced Rotorcraft Technology and Disaster Relief, Gifu, Japan, April 21-23, 1998.

[6] Kitaplioglu, C., "Blade–Vortex Interaction Noise of a Full Scale XV-15 Rotor Tested in the NASA Ames 80- by 120-Foot Wind Tunnel, "NASA TM 1999-208789, July 1999.

[7] Kitaplioglu, C., McCluer, M., and Acree, C.W., "Comparison of XV-15 Full-Scale Wind Tunnel and In-Flight Blade-Vortex Interaction Noise," American Helicopter Society 53rd Annual Forum, Virginia Beach, VA, April 1997.

[8] Kitaplioglu, C and Betzina, M and Johnson, W., "Blade-Vortex Interaction Noise of an Isolated Full-Scale XV-15 Tiltrotor," American Helicopter Society 56th Annual Forum, Virginia Beach, VA, May 2-4, 2000.

[9] Barbely, N., Kitaplioglu, C., and Sim, W., "Acoustics Reflections of Full-Scale Rotor Noise Measurements in NFAC 40-by 80-Foot Wind Tunnel," American Helicopter Society Specialists' Conference, San Francisco, CA, January 20-21, 2012.

[10] "GRAS Measurement Microphone Sets." GRAS, www.gras.dk/products/measurement-microphone-sets.

[11] Kinsler, L.E., Frey, A.R., Coppens, A.B. and Sanders, J.V., "Fundamentals of Acoustics," 4th Edition. ISBN 0-47184789-5. Wiley-VCH, December 1999.